Macromolecules

Volume 37, Number 12 June 15, 2004

Communications to the Editor

Molecular Dynamics Study of the Evaporation Process in Polymer Films

Mesfin Tsige* and Gary S. Grest*

Sandia National Laboratories, Albuquerque, New Mexico 87185

Received March 11, 2004
Revised Manuscript Received April 27, 2004

The wide range of applications of thin polymer films in electronics, coating, and biomedicine[1−5] have attracted much interest in recent years. These applications usually require the film to be homogeneous, of uniform thickness, and stable. Thin polymer films often have different properties compared to bulk materials. Due to the high viscosity of polymer melts, in many cases the polymer is first dissolved in a low viscosity solvent, the solution is then spread on the substrate and the solvent subsequently evaporates. Spin coating is one technique that is often used for preparing thin polymer films on a solid substrate. A wide range of film thicknesses usually with uniform thickness and low surface roughness can be prepared using this technique. Other techniques include dip coating from solution and solution casting. Some of the factors which control the film thickness and surface roughness of the films directly after preparation have been studied. The solution concentration and viscosity and the solvent evaporation rate[2−4,6] are important parameters for controlling film thickness, whereas the rate of solvent evaporation[2,3] is important for controlling surface roughness.

How the solvent evaporation process affects the structure of the film is not well understood. Bornside et al.[1] developed a one-dimensional model of the spin coating process and made several important predictions regarding the mechanisms of flow and evaporation during spin coating. This model predicted that the region near the free surface becomes polymer rich first due to solvent evaporation, though this has not been verified experimentally. de Gennes[5] argued that for glassy polymer films this polymer rich region is under mechanical tension, which could lead to cracks in the film. For nonglassy polymer films when the surface tension of the solvent is smaller than that of the polymer, de Gennes[7] predicted a minimum value of the film thickness, which depends on the rate of solvent evaporation, for the onset of an instability in the thin film due to concentration gradients. On the other hand, Okoroanyanwu[8] showed that instabilities also exist in ultrathin films (<53 nm) deposited onto silicon wafer substrates due to interfacial effects, cooperative dynamics, and perhaps polymer chain packing constraints.

Table 1. Parameter for the Three Different Systems Studied[a]

system	M/N_p	c_0	N_T	T_t/τ	L_x/σ	L_z^i/σ
I	100/1000	0.80	5×10^5	8.1×10^4	100	81.4
II	300/1000	0.25	4×10^5	8.0×10^4	100	58.2
III	600/500	0.50	6×10^5	4.3×10^5	60	224.3

[a] M is the number of polymer chains of chain length N_p, c_0 is the initial mole fraction of solvent within the system, $N_T = MN_p + N_s$ is the total number of monomers, T_t is total time of run, $L_x = L_y$ are the surface dimensions, and L_z^i is initial film thickness.

With recent advances in parallel molecular dynamics (MD) algorithms and increased computational power, it is now possible to study one important aspect of this progress, namely the evaporation process. In this paper, we present results from the first large-scale simulation of solvent evaporation from a solvent−polymer solution. Our study focuses on the morphology of the thin film during the solvent evaporation process.

We perform MD simulations of coarse grained models of solvent−polymer mixtures. The polymers are represented by freely jointed bead spring chains of length N_p monomers of mass m, and the solvent is modeled as single monomers. Here $N_p = 500$ or 1000 (see Table 1).

* To whom correspondence should be addressed. E-mail: mtsige@sandia.gov (M. T.); gsgrest@sandia.gov (G.S.G.).

10.1021/ma049509v CCC: $27.50
Published on Web 05/14/2004

Nonbonded pairs of monomers interact through the standard Lennard-Jones 12-6 potential

$$U_{\mathrm{LJ}}(r) = \begin{cases} 4\epsilon\left\{\left(\frac{\sigma}{r}\right)^{12} - \left(\frac{\sigma}{r}\right)^{6}\right\} + \epsilon_{\mathrm{LJ}}, & r \le r_{\mathrm{c}} \\ 0, & r > r_{\mathrm{c}} \end{cases} \quad (1)$$

where r is the distance between monomers and ϵ_{LJ} is a constant added so that the potential is continuous at $r = r_{\mathrm{c}}$. Here we take $r_{\mathrm{c}} = 2.5\sigma$. The basic unit of time is $\tau = \sigma(m/\epsilon)^{1/2}$, and the energy scale is set by ϵ. Bonded monomers have an additional anharmonic interaction potential known as the FENE potential.[9,10] The interaction parameters are chosen to prevent chain crossing and are the same as in ref 10.

We have studied three different systems that are listed in Table 1. The systems differ by the number of solvent particles, number of polymer chains, and polymer chain length. Very high solvent concentration is usually used in spin coating, but due to computational limitations the maximum solvent concentration studied is 0.8. Periodic boundary conditions are used in the x and y directions, and the solvent evaporates in the z direction. Initially solutions were placed between two flat surfaces at the separation L_z^i shown in Table 1. The systems were equilibrated at pressure $P \simeq 0$ and temperature $T = \epsilon/k_{\mathrm{B}}$. The monomer-surface interaction for systems I and II is given by the 10-4 LJ potential[11] and for system III is given by the 9-3 LJ potential, both with a cutoff distance $r_{\mathrm{c}}^{\mathrm{w}} = 2.2\sigma$.[12] The surface strength is chosen to be strong enough that a vapor phase[13] did not form between the polymer and the wall. The top surface is then removed so that the solution is in contact with a vacuum. As the solvent monomers evaporate, they are removed from the system when they reach a specified distance above the original film, typically 50σ. The distance at which vapor monomers are extracted has no effect on the evaporation process. Due to the relatively small surface area of the films, 3600 and $10^4\sigma^2$, we do not expect to see any instabilities[7,8] during the evaporation process. Note that for a polymer melt of long fully flexible chains the glass transition temperature is $T_{\mathrm{g}} = 0.5 - 0.6\epsilon/k_{\mathrm{B}}$.[14] Hence, our systems, in the limit of no solvent, are well above the glass transition.

System III was run using the massively parallel grand canonical MD code LADERA[15] which is a hybrid of the massively parallel MD code LAMMPS[16] and a grand canonical MC code,[17] whereas systems I and II were run using our shared memory MD code. The equations of motion were integrated with a velocity−verlet algorithm with a time step of $\Delta t = 0.009\tau$ for systems I and II and $\Delta t = 0.01$ for system III. The simulations were performed at constant temperature T using the Langevin thermostat with damping constant $\gamma = 0.5/\tau$ and were run until at least 90% of the solvent had evaporated. For system III, this took a very long run of about $4.3 \times 10^7\Delta t$ as reported in Table 1. The average radius of gyration and end-to-end distance of the polymer chains in the systems decreased as the solvent evaporated.

Figure 1 shows the density profiles of polymer and solvent for system III as a function of time, with initial solvent fraction $c_0 = 0.5$. The substrate is at $z = 0$. The density at a given value of z, $\rho_i(z)$, is calculated by partitioning the system volume into bins along the z direction and counting the number of type i monomers in each bin per partitioned volume. Due to evaporation, the solvent density in the system decreases as a function of time, whereas the density of the polymer increases to its melt density value ($\rho \simeq 0.8\sigma^{-3}$) by reducing the film thickness. One important point to notice in the evaporation process is the sharp increase in polymer density at the film/vapor interface which creates a polymer density gradient across this interface. This polymer density gradient becomes a barrier to solvent evaporation and results in a solvent density gradient within the system. A similar solvent evaporation effect was also observed for system I as shown in Figure 2. Since the polymer is initially much more dilute ($c_0 = 0.80$) the immediate increase in polymer density across the interface is not as sharp as in system III but there is still a polymer density gradient across the interface. For system II, the dilute solvent case (not shown here), there is only a small polymer density gradient across the interface since the polymer density within the system is already close to the pure polymer melt density. The difference in the density gradient across the interface in the three different systems results in different solvent evaporation rates.

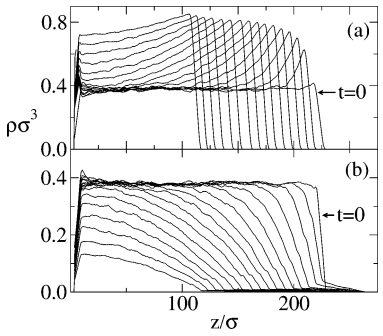

Figure 1. Time evolution of the density profile in the solvent evaporation direction for (a) polymer and (b) solvent during the evaporation process in system III. The profiles are at different times and from right to left corresponds to $t/(10^3\tau) =$ 0, 4, 10, 20, 30, 40, 60, 80, 100, 140, 180, 220, 260, 310, 360, and 430. The substrate is at $z = 0$.

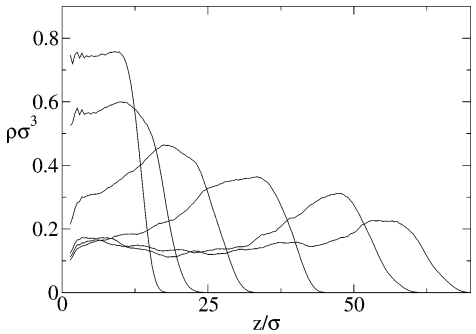

Figure 2. Polymer density profiles for system I at different times in the evaporation process. The profiles from right to left corresponds to $t/(10^3\tau) = 4.5$, 9, 18, 27, 36, and 45. The substrate is at $z = 0$.

Figure 3a shows the concentration of solvent monomers c remaining in the film divided by the initial solvent concentration c_0. The rate of solvent evaporation in system III (circles) is clearly much slower than the other two systems. This may be in part due to the difference in the thickness of the films. System II (squares) with dilute solvent and system III with intermediate solvent concentrations show an exponential solvent evaporation. System I, however, shows two distinct solvent evaporation behaviors: initially showing a similar evaporation rate as system II but then changing to a higher evaporation rate. This can be

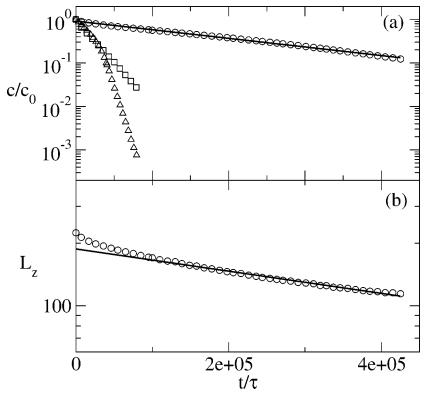

Figure 3. Logarithmic plot of (a) the concentration of solvent remaining in the film divided by its value at $t = 0$ in system I (triangles), system II (squares), and system III (circles), (b) film thickness versus time for system III. The solid line in both (a) and (b) is an exponential fit to the data.

explained by the polymer density profile shown in Figure 2. In that case, there is a polymer density gradient across the interface which slows the solvent evaporation from the system. Then, though the polymer density at the interface ($0.6\sigma^{-3}$) is still far from the melt density value ($0.8\sigma^{-3}$), the polymer density gradient, i.e., the barrier to solvent evaporation, disappears resulting in an increase of solvent evaporation.

The film thickness is also found to decrease exponentially as shown in Figure 3b. The film thickness L_z is defined as the average height of the film at time t/τ. The width of the interface, measured from the fluctuation in film thickness, is constant with time. This is expected since the simulations are done far above the glass transition temperature and the polymer film is fluid like. The final roughness of the films is due to an intrinsic width which depends on the liquid−vapor surface tension and a capillary wave contribution which increases logarithmically with surface area.[13,18,19] The question of roughness and film instability are usually an issue for glassy polymers or if the solvent has been used as a plasticizer.

In summary, we performed large-scale MD simulations to study the morphology of polymer films during solvent evaporation. The density profile of the solvent and polymer has been calculated from the simulations as a function of time. The formation of a polymer density gradient at the film/vapor interface has been observed. The rate of solvent evaporation from the film is found to depend strongly on the magnitude of this density gradient. The magnitude of the density gradient depends on time and also on solvent concentration in the system.

Acknowledgment. Sandia is a multiprogram laboratory operated by Sandia Corporation, a Lockheed Martin company, for the United States Department of Energy's National Nuclear Security Administration under Contract No. DE-AC04-94AL85000.

References and Notes

(1) Bornside, D. E.; Macosko, C. W.; Scriven, L. E. *J. Appl. Phys.* **1989**, *66*, 5135.
(2) Strawhecker, K. E.; Kumar, S. K.; Douglas, J. F.; Karim, A. *Macromolecules* **2001**, *34*, 4669.
(3) Müller-Buschbaum, P.; Gutmann, J. S.; Wolkenhauer, M.; Stamm, M.; Smilgies, D.; Petry, W. *Macromolecules* **2001**, *34*, 1369.
(4) Mellbring, O.; Oiseth, S. K.; Krozer, A.; Lausman, J.; Hjertberg, T. *Macromolecules* **2001**, *34*, 7496.
(5) de Gennes, P. G. *Eur. Phys. J. E* **2002**, *7*, 31.
(6) Müller-Buschbaum, P.; Gutmann, J. S.; Lorenz, C.; Schmitt, T.; Stamm, M. *Macromolecules* **1998**, *31*, 9265.
(7) de Gennes, P. G. *Eur. Phys. J. E* **2001**, *6*, 421.
(8) Okoroanyanwu, U. *J. Vac. Sci. Technol. B* **2000**, *18*, 3381.
(9) Grest, G. S.; Kremer, K. *Phys. Rev. A* **1986**, *33*, 3628.
(10) Kremer, K.; Grest, G. S. *J. Chem. Phys.* **1990**, *92*, 5057.
(11) Grest, G. S. *J. Chem. Phys.* **1996**, *105*, 5532.
(12) Sides, S. W.; Grest, G. S.; Stevens, M. J. *Macromolecules* **2002**, *35*, 566.
(13) Sides, S. W.; Grest, G. S.; Lacasse, M. D. *Phys. Rev. E* **1999**, *60*, 6708.
(14) Baljon, A. R. C.; Robbins, M. O. *Macromolecules* **2001**, *34*, 4200.
(15) Thompson, A. P.; Heffelfinger, G. S. *J. Chem. Phys.* **1999**, *110*, 10693.
(16) Plimpton, S. J. *J. Comput. Phys.* **1995**, *117*, 1.
(17) Heffelfinger, G. S.; van Swol, F. *J. Chem. Phys.* **1994**, *100*, 7548.
(18) Sanyal, M. K.; Sinha, S. K.; Huang, K. G.; Ocko, B. M. *Phys. Rev. Lett.* **1991**, *66*, 628.
(19) Hapke, T.; Päzold, G.; Heermann, D. W. *J. Chem. Phys.* **1998**, *109*, 10075.

MA049509V